Articles

X-ray Structure and Catalytic Mechanism of Lobster Enolase†

Stéphane Duquerroy,‡ Christelle Camus,§ and Joël Janin*,‡

Laboratoire de Biologie Structurale, UMR 9920 CNRS, Université Paris-Sud, 91198 Gif-sur-Yvette, France, and Laboratoire Information Génétique et Développement, URA 1354 CNRS, Université Paris-Sud, 91405-Orsay Cedex, France

Received May 5, 1995; Revised Manuscript Received June 28, 1995⊗

ABSTRACT: Enolase prepared from lobster tail muscle yielded trigonal crystals with one 47 kDa subunit per asymmetric unit. X-ray data were collected on the apoenzyme at 2.4 Å resolution and on a complex with Mn^{2+} and the inhibitor phosphoglycolate at 2.2 Å resolution. The corresponding cDNA was amplified from a library of lobster muscle cDNA, and a sequence corresponding to residues 27−398 was determined. It is highly homologous to other enolases, including yeast enolase for which an X-ray structure is available. Yeast enolase was used as a starting point for crystallographic refinement, which led to models of lobster enolase having *R*-factors below 22% and good stereochemistry. These models are very similar to yeast enolase; they have the same fold with a $\beta_3\alpha_4$ N-terminal domain followed by an atypical α/β barrel. Lobster apoenolase and the ternary complex differ only in the position of three mobile loops. In the complex, a single Mn^{2+} ion is seen ligated to three carboxylates and three water molecules. Phosphoglycolate binds near, but not directly to, the metal. His 157, which belongs to one of the mobile loops, is in contact with the C_2 atom of the ligand. A water molecule hydrogen-bonds to the carboxylate of the ligand and to those of Glu 166 and Glu 209. We suggest that His 157 is the base that abstracts the C_2H proton, whereas the water molecule is part of a proton relay system keeping the substrate in the carboxylic acid form where the pK_a of the C_2H group is low enough for proton transfer to His 157. The resulting catalytic mechanism is different from those proposed on the basis of the yeast enzyme X-ray structures, but it fits with earlier biochemical and spectroscopic data.

Enolase catalyzes the reversible dehydration of 2-phospho-D-glycerate to phosphoenolpyruvate as part of the glycolytic and gluconeogenesis pathways (Wold, 1971). The reaction requires divalent cations, Mg^{2+} being the activating metal under physiological conditions whereas Zn^{2+} or Mn^{2+} are active *in vitro*. Enolases from various organisms are dimers with identical subunits of about 47 kDa. Each subunit binds a divalent ion in the absence of substrate and a second ion in its presence. The two metal sites, which have been called conformational and catalytic in the past, are referred to below as sites I and II since both are involved in catalysis (Lee & Nowak, 1992a). The mechanism originally proposed for the reaction involves the abstraction of the proton carried by the C_2 atom of phosphoglycerate (**1**), yielding the carbanion **2** and followed by β-elimination of the hydroxyl group on C_3 (Dinovo & Boyer, 1971). Hydration of phosphoenolpyruvate (**3**) goes through the same steps in reverse. This mechanism raises several questions. First, the carbon acid has a high pK_a and the hydroxyl is a poor leaving group. Second, what is the base that takes up the proton and what role do the metal ions play?

These questions have received contradictory answers on the basis of chemical, spectroscopic, and structural data.

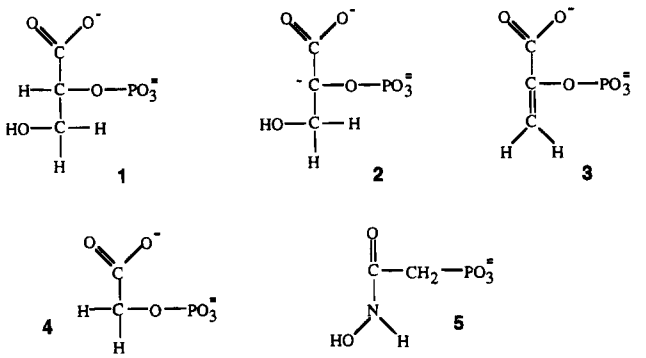

Yeast enolase is the only one for which an X-ray structure is available. The fold of the polypeptide chain was first determined by Lebioda and Stec (1988) and Stec and Lebioda (1990). It contains an α/β barrel of an unusual type, with a topology that differs from the one commonly observed in triose-phosphate isomerase (Banner et al., 1975) and many other proteins. Details of the yeast enolase active site have been established in further X-ray structures of complexes with a variety of divalent ions, the substrates, or the inhibitor phosphoglycolate (**4**) (Lebioda & Stec, 1989, 1991; Lebioda et al., 1989, 1991). These data led to the proposal that the catalytic base is a water molecule activated by two glutamates and that the metal at site I ligates the hydroxyl on the substrate and promotes β-elimination. In these studies, the location and role of metal site II were unclear. More recently, two X-ray structures of yeast enolase in complex with the high-affinity inhibitor phosphonoacetohydroxamate

† Atomic coordinates have been deposited at the Brookhaven Protein Data Bank and are listed under file names 1PDY and 1PDZ.

* To whom correspondence should be addressed (fax 33.1.69 82 31 29; e-mail janin@cygne.lbs.cnrs-gif.fr).

‡ Laboratoire de Biologie Structurale.

§ Laboratoire Information Génétique et Développement.

⊗ Abstract published in *Advance ACS Abstracts,* September 1, 1995.

0006-2960/95/0434-12513$09.00/0

(**5**) were established in the presence of either Mg^{2+} (Wedekind et al., 1994) or Mn^{2+} (Zhang et al., 1994). These structures lead to different interpretations fostering opposite views on the location of metal site II, the nature of the catalytic base, and the role of the metals.

We report here the amino acid sequence of lobster enolase derived from a cDNA sequence, the X-ray structure of the apoenzyme at 2.4 Å resolution, and that of a ternary complex with Mn^{2+} and phosphoglycolate at 2.2 Å resolution. The lobster protein is a dimer made of 433 residue subunits with a sequence that is highly homologous to other enolases. The chain tracing, initially done in a SIRAS electron density map (Dumas et al., 1995), is closely similar to that of the yeast enzyme. The structure of the active site that we observe in the Mn^{2+}−phosphoglycolate complex is in general agreement with available data on yeast enolase as far as metal site I and the substrate site are concerned. We agree with Lebioda and collaborators and differ from Wedekind et al. (1994) on the role of the metal at site I. We differ from Lebioda and collaborators on the nature of the catalytic base. We suggest that it is a histidine and that, instead of being a base, the water molecule identified by Lebioda and Stec (1991) at the active site acts as an acid catalyst to protonate the carboxylate of 2-phosphoglycerate and lower the pK_a of its α-proton to a value compatible with the observed rate of catalysis.

MATERIALS AND METHODS

Amplification and Sequence of the Lobster Enolase cDNA. The cDNA library constructed by Dumas and Camonis (1993) from lobster muscle polyadenylated mRNA was examined for the presence of enolase cDNA. In this library, oligo(dT)-primed cDNAs were inserted at the unique cloning site *Eco*RI of bacteriophage λgt11. The library was plated out at high plaque density (10^5 pfu/plate) with *Escherichia coli* Y1090 as the host strain (Sambrook et al., 1989). Confluent lysis was reached after 6−8 h of incubation at 37 °C. Bacteriophage particles were resuspended in SM buffer and purified by overnight sedimentation at 4000*g* and 4 °C. Purified DNA was subjected to PCR amplification with *Taq* polymerase from Appligene. Two degenerated oligonucleotide primers were chosen on the basis of peptide sequences: ASTGVHEA starting at position 38 in the forward direction and QIKTGAP at position 393 in the reverse direction. These peptides are present in all known enolase sequences. The primers were (1) 5′-GCITCCACTGGYRTYYAYGARGC-3′ and (2) 5′-GGRGCACCAGTCTTGATCTG-3′. Y is a pyrimidine, R, a purine, and I, inosine matching any of the four bases. Forty cycles were completed in the Perkin-Elmer PCR apparatus as follows: melting at 92 °C for 1 min, annealing at 50 °C for 1 min, and chain extension at 72 °C for 2 min.

The amplified DNA fragment covers 83% of the enolase coding sequence. It was labeled with the ECL kit (Amersham) and used as a probe to isolate cDNA clones from the λgt11 library. As we failed to isolate positive clones, the sequence was directly determined on PCR-amplified DNA. The product of three distinct amplifications was subjected to automatic sequencing using dye dideoxy terminators in the Applied Biosystems 373A apparatus. Nucleotide sequences were assembled and translated using the GCG package (Devereux et al., 1984). Lobster enolase was compared to other enolases using the Bestfit, Pileup, and Pretty programs in this package.

Table 1: X-ray Data Collection and Model Refinement

	apoenolase	complex
data collection resolution (Å)	2.4	2.2
observed intensities	78769	97010
unique reflections	19309	27950
completeness (%)	91.4	97.5
reflections with $I > 3\sigma$ (%)	72.5	81.1
	46.5 (2.5−2.4 Å)	43.1 (2.3−2.2 Å)
R_{merge}[a] (%)	7.7	7.4
	35.3 (2.5−2.4 Å)	39.3 (2.3−2.2 Å)
refinement		
resolution range (Å)	20.0−2.4	20.0−2.2
R-factor	21.5	21.7
protein atoms	3300	3300
solvent molecules	109	119
rmsd from ideal values		
bond lengths (Å)	0.007	0.010
bond angles (deg)	1.38	1.60
χ_1 dihedral angles (deg)	23.1	23.4
improper dihedrals (deg)	1.28	1.46
temperature factors (Å^2)		
main-chain atoms	31.1	36.4
side-chain atoms	33.9	39.2
phosphoglycolate (50% occ)		29.7
Mn^{2+} ion		42.2

[a] $R_{merge} = \sum|I(h)_i - \langle I(h)\rangle|/\sum I(h)_i$.

Crystallography. Enolase was prepared from lobster tail muscle as reported previously (Duquerroy et al., 1994). Crystals (0.3 mm^3) were grown at 16 °C by the hanging drop method in HEPES buffer (50 mM, pH 7.6) and 2.5−2.7 M ammonium sulfate. They belong to trigonal space group $P3_121$ with unit cell dimensions $a = b = 110.8$ Å, $c = 73.4$ Å, $\alpha = \beta = 90°$, $\gamma = 120°$, and one molecule per asymmetric unit. X-ray data were collected on native crystals and a mercury derivative (Dumas et al., 1995). In addition, a complex with Mn^{2+} and the inhibitor phosphoglycolate was obtained by soaking in 10 mM $MnCl_2$ and 20 mM inhibitor for 12 h. All data were taken at 4 °C at the W32 station (Fourme et al., 1992) of the LURE-DCI synchrotron center (Orsay, France) on a 180 mm imaging plate system (Mar-Research, Hamburg). The wavelength was set to 0.91 Å. Intensities were evaluated with MOSFLM (Leslie et al., 1986), and further processing used the CCP4 program suite (CCP4, Daresbury Laboratory, Warrington, U.K.). A summary of data collection statistics is given in Table 1.

As reported, enolase was initially crystallized as a contaminant of arginine kinase (Duquerroy et al., 1994), and much of the crystallographic study was completed before the protein was identified as enolase by peptide sequencing. Thus, the polypeptide chain was partly traced in the SIRAS electron density map modified by solvent flattening (Dumas et al., 1995). After it was recognized to be an enolase, the atomic model of yeast enolase (Lebioda et al., 1989) could be placed directly in the SIRAS map by overlapping secondary structure elements present in the partial model. After rigid body refinement, the yeast model had a *R*-factor of 41.7% against our 4.0 Å diffraction data. Further model building was performed with graphic program O (Jones et al., 1991) in combined electron density maps calculated with reduced-bias coefficients according to the SIGMAA scheme (Read, 1986). Sequence information was introduced and refinement carried out with X-PLOR (Brünger et al., 1987) using parameters for ideal stereo-

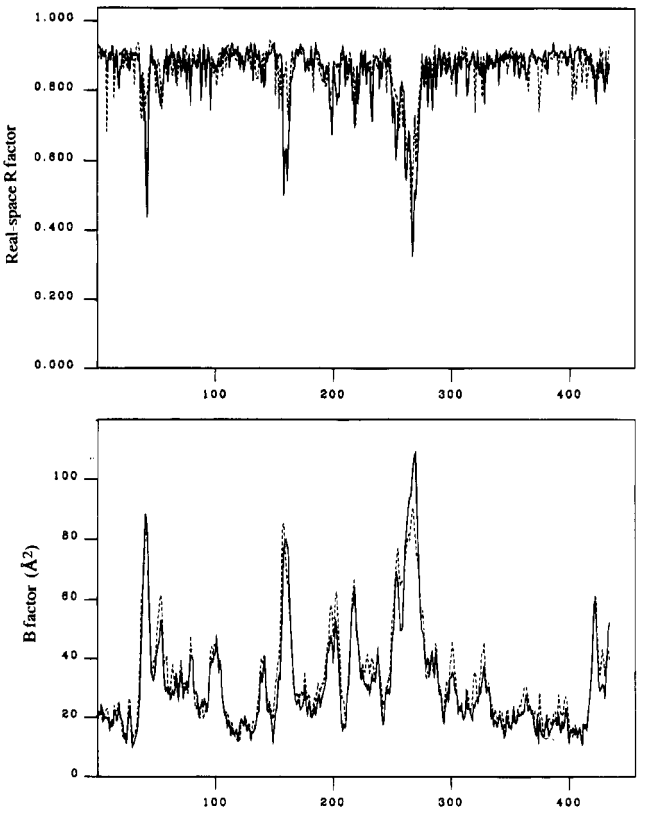

FIGURE 1: Direct-space *R*-factor and temperature factors. (a, top) Direct-space factor of agreement between observed and calculated electron density in apoenolase (full line) and in the Mn^{2+}–phosphoglycolate complex (dashes) as determined with program O (Jones et al., 1991). Average values are 0.86 (apo) and 0.87 (complex), respectively. (b, bottom) Main-chain *B*-factors for the two refined models.

chemistry from Engh and Huber (1991). Three poorly ordered regions of the atomic model (residues 37–43, 155–162, and 251–273) were omitted from initial stages of refinement. In these regions, the correlation between observed and calculated electron densities remained lower than average and main-chain isotropic temperature factors higher than average even after refinement (Figure 1), but the main chain had unambiguous density everywhere except for residues 263–271.

Final statistics for the two models of unligated lobster enolase (apoenolase) and the Mn^{2+}–phosphoglycolate complex are given in Table 1. The models include all 433 residues of the amino acid sequence, 109 solvent molecules and a sulfate ion for apoenolase, 119 solvent molecules, a fully occupied Mn^{2+} ion, and a phosphoglycolate molecule with 50% occupancy for the complex. They have *R*-factors less than 22% and an excellent stereochemistry based on departure from ideal bond lengths and angles. More than 85% of the (ϕ,ψ) pairs lie in the most favored regions of the Ramachandran plot (Laskowski et al., 1993). In both models, one non-glycine residue (Arg 401) lies at the edge of permitted regions.

RESULTS AND DISCUSSION

The Sequence of Lobster Enolase. The amino acid sequence of lobster enolase was derived from the PCR-amplified cDNA sequence for residues 38–398 as described above. Residues 27–37 were known from previous peptide sequencing (Duquerroy et al., 1994). The missing N-terminal residues 1–26 and C-terminal residues 399–433 were assigned by homology with other known enolase sequences, taking the electron density map as a control. All enolases are highly homologous, with more than 60% pairwise identity between eukaryotic enolases. Within residues 28–398, lobster enolase is 64% identical to yeast enolase with a gap of two residues near position 143 and an insertion of one at position 256. The whole sequence is 78% identical to *Drosophila* enolase, its closest relative and the only other one that is available from an arthropode.

The sequences listed in Figure 2 for residues 1–26 and 399–433 are therefore likely to be correct at all but a few of 60 positions, of which only Ser 13 is near the active site. The fit to the electron density is as good for the homology-derived N- and C-terminal sequences as it is in the best parts of the map for the cDNA-derived sequence. An example is the N-terminal residue, which chemical sequencing showed to be blocked. It was therefore taken to be an acetylated serine like in yeast or rabbit muscle enolases (Wold, 1971), in full agreement with the density (Figure 3). No other posttranslational modification was detected in the electron density map.

The Enolase Fold. The three-dimensional structure of lobster enolase shown in Figure 4 is very similar to that of the yeast enzyme (Stec & Lebioda, 1990). The root-mean-square distance (rmsd) between C_α positions in subunits of the two enzymes is 0.83 Å for all residues excluding 268–270. This is the value expected for two sequences that share 64% identity (Chothia & Lesk, 1986). Residues 268–270, where the discrepancy reaches 6 Å, are part of a large external loop (called L3 below) which is poorly ordered in both structures. Lesser discrepancies are found near the C-terminus at residues 420–430.

The lobster enolase dimer associates in the same way as the yeast enzyme. The two subunits are related by crystallographic 2-fold symmetry. Subunit contacts in the dimer bury 3740 Å^2 of the protein surface, or 12% of its solvent accessible surface. The subunit interface is large for a dimeric protein (Janin et al., 1988), and we have no evidence for a monomeric species of lobster enolase in solution, whereas yeast enolase has been reported to dissociate at low concentration and in the absence of divalent ions (Brewer, 1981).

Elements of secondary structure listed in Table 2 are the same as in yeast. The subunit folds in two well-defined domains. Residues 1–140 form the N-terminal domain. It comprises a three-stranded antiparallel β-sheet (strands (β_a–β_c) followed by loop L1 and four α-helices, α_a–α_d, a topology which we can write $\beta_3\alpha_4$. The remainder of the polypeptide chain is an α/β barrel with an eight-stranded β-sheet surrounded by helices α_1–α_8. The barrel has additional β-strands marked β_e–β_k inserted after helix α_1, after strand β_3, and at the C-terminus. It resembles the classical α/β barrel of triose-phosphate isomerase (Banner et al., 1975; Farber, 1993), but strand β_2 runs antiparallel to the other seven strands and helix α_1 to the other seven helices. The β_1–β_2 connection is made by loop L2, and helices α_1–α_2 form a hairpin connecting strands β_2 and β_3. The topology of the barrel is therefore $(\beta\beta\alpha\alpha)(\beta\alpha)_6$ rather than $(\beta\alpha)_8$ as in classical α/β barrels. This peculiarity unique to enolase is now confirmed by the structure of the lobster enzyme.

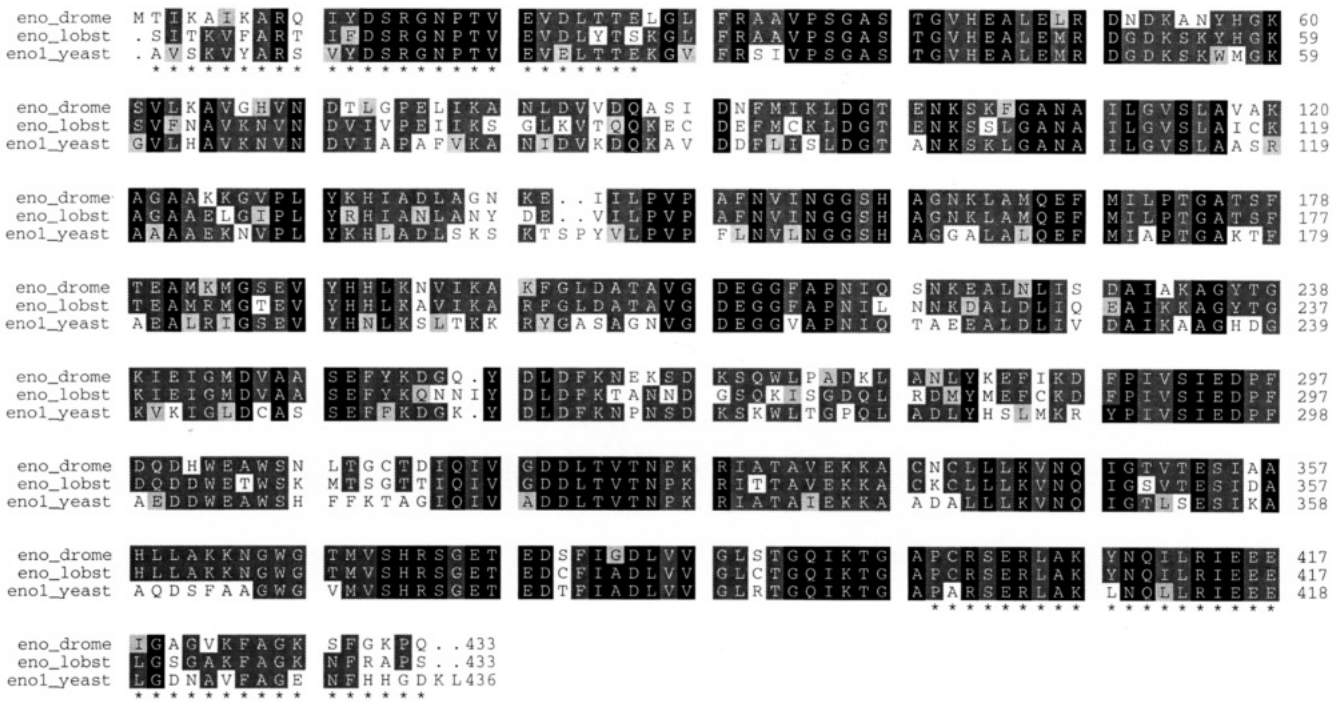

FIGURE 2: Alignment of enolase sequences. The sequence used in the crystallographic model is compared with those from yeast (Holland et al., 1981) and *Drosophila melanogaster* (Bishop & Corces, 1990). The lobster sequence was obtained by peptide sequencing for residues 26−37 and by cDNA sequencing for residues 38−398. It was derived by homology and inspection of the electron density map for residues 1−25 and 399−433 (stars). Identical residues in these three sequences are shaded; black indicates residues that are identical in all but 2 of 27 enolase sequences including prokaryotes and one archaebacterium.

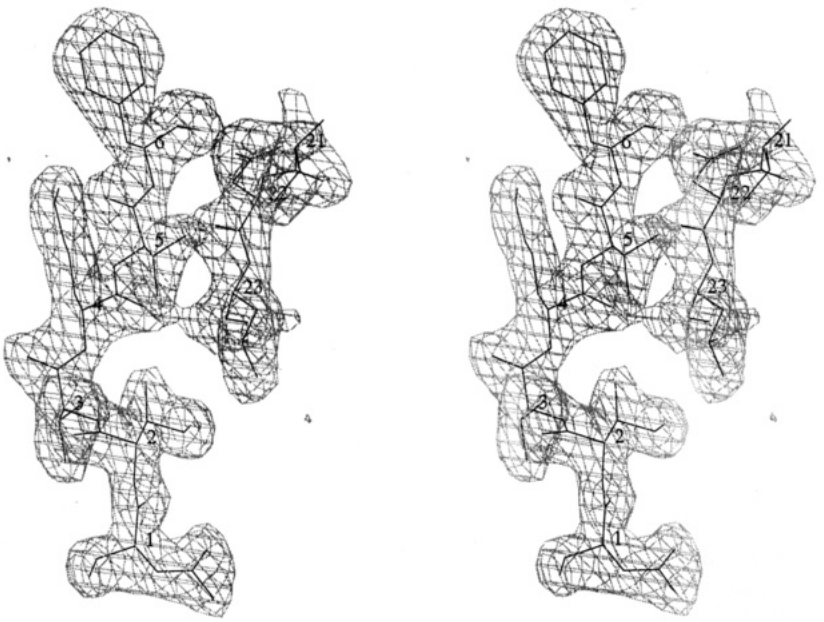

FIGURE 3: Electron density in the N-terminal region. $2F_o - F_c$ map contoured at 1σ for residues 1−6 and 21−23, the sequence of which was assigned by homology. The blocked N-terminus was interpreted as acetylserine. Drawn with program O (Jones et al., 1991).

Conformation Changes upon Binding Mn^{2+} and Phosphoglycolate. The X-ray structure of the ternary complex was obtained by diffusion of Mn^{2+} and phosphoglycolate in crystals. The metal and inhibitor bind close to each other in a cavity located at the C-terminal end of the β-barrel and at the interface of the two domains (Figure 5). Their location corresponds to the description of the active site in yeast enolase given by Lebioda and Stec (1991). Binding takes place with no major conformation change or subunit or domain movement as shown by the rmsd. It is 0.61 Å for all C_α's, but this figure includes 22 residues in three loops that undergo main-chain movements larger than 1 Å. Omitting these residues, the rmsd is 0.26 Å for C_α and 0.65 Å for all atoms, of the order of experimental errors.

The mobile loops are L1 (residues 36−43) in the N-terminal domain, L2 (residues 155−164) connecting antiparallel strands β_1 and β_2 of the α/β barrel, and L3 (residues 258−271), part of a larger insertion between β_3 and α_3. All three loops have high temperature factors in both structures, and they are also mobile in the yeast enzyme (Lebioda & Stec, 1990). L1 and L2 are located near the active site, and they move by 1−3 Å toward it in the complex. Thus, their repositioning is likely to be significant for the function. In yeast enolase, a movement of these two loops occurs upon

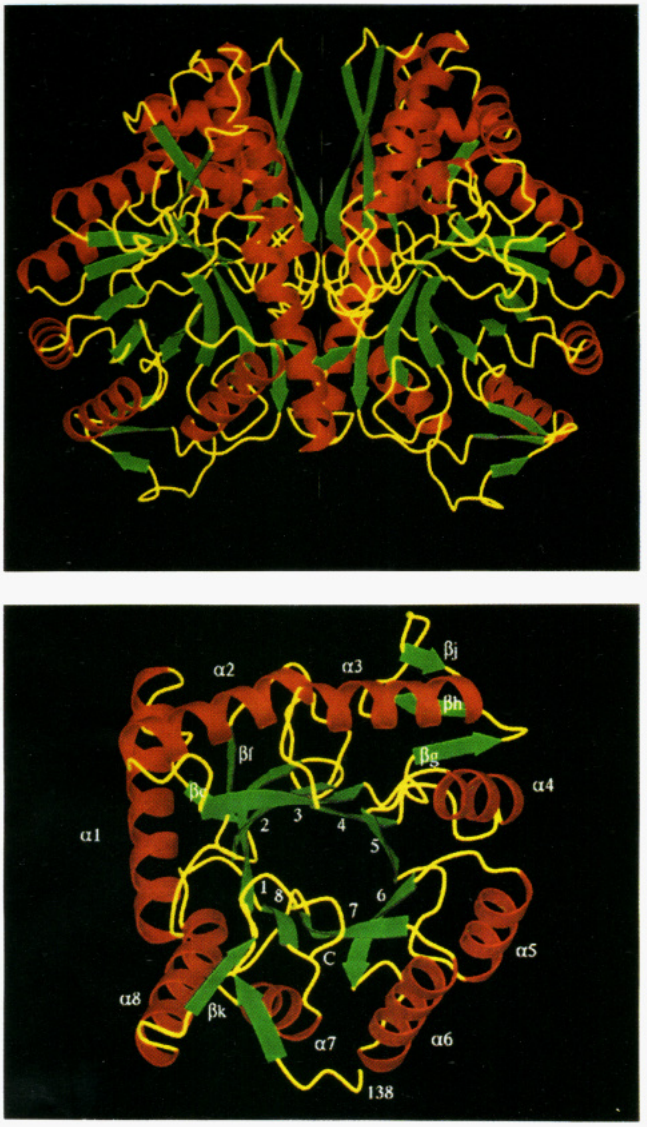

FIGURE 4: Lobster enolase. (a, top) The dimer. The 2-fold axis is dashed. (b, bottom) The α/β barrel (residues 138−433). Note the peculiar $\beta\beta\alpha\alpha(\beta\alpha)_6$ topology, which is unique to enolase. Drawn with Molscript (Kraulis, 1991).

binding metal alone (Lebioda et al., 1989; Lebioda & Stec, 1989; Wedekind et al., 1995) or metal and a substrate or inhibitor (Lebioda et al., 1991; Lebioda & Stec, 1991; Zhang et al., 1994; Wedekind et al., 1994). L3 is on the protein surface, remote from the active site, and it plays no role in binding the metal or the inhibitor. Its movement from one lobster enolase X-ray structure to another is large (up to 5 Å) but most likely of no functional importance, since equally large differences are observed between the unligated lobster and yeast enzymes.

Metal Site I and the Active Site. In the ternary complex, the highest electron density peak (6σ) corresponds to a Mn^{2+} ion with nearly full occupancy. The metal has octahedral coordination to the oxygens of three carboxylates and three water molecules (Table 3 and Figure 6). The carboxylates belong to residues Asp 244, Glu 294, and Asp 319. These residues are located at the C-terminal end of respectively strands β_3, β_4, and β_5 in the α/β barrel. Bond lengths are in the 2.0−2.4 Å range expected for metal−oxygen bonds. This metal site is identical to the one reported for yeast enolase in a binary complex with either Zn^{2+} (Lebioda & Stec, 1989) or Mg^{2+} (Wedekind et al., 1995) and in a ternary complex

Table 2: Secondary Structure

main features		additional elements	
N-terminal domain			
β_a	4−12	type I turn	12−15
β_b	16−25	type I turn	25−28
β_c	28−34	loop L1	36−43
α_a	61−80	type I turn	82−85
α_b	85−98	type I turn	99−102
		type I turn	103−106
α_c	107−125		
α_d	129−137	type I turn	139−142
α/β barrel			
β_1	142−154	loop L2	155−164
β_2	165−172	type I turn	171−174
α_1	175−199	β_e	204−207
		type I turn	207−210
		β_f	211−214
α_2	217−234	type II turn	235−238
β_3	240−245	type I turn	246−249
		β_g	250−252
		type II turn	253−256
		β_h	256−258
		loop L3	259−270
		β_j	271−272
α_3	274−288	γ turn	288−290
β_4	290−295	type VIII turn	295−298
		type I turn	298−301
α_4	301−312		
β_5	315−318	type I turn	320−323
		type I′ turn	322−325
α_5	325−335		
β_6	339−343		
α_6	344−364		
β_7	367−372	type VIII turn	373−376
α_7	380−389		
β_8	392−395	γ turn	398−400
α_8	401−419	β_k	423−426

with Mg^{2+} and substrate (Lebioda & Stec, 1991). As it can be occupied in the absence of the substrate, it must correspond to site I of biochemical and spectroscopic studies (Lee & Nowak, 1992b) and the metal environment fits with expected properties of site I.

The phosphoglycolate molecule is at the active site of lobster enolase in the vicinity of the metal (Figure 7). Both the density and the results of temperature factor refinement indicate that the site is not fully occupied under the conditions we have used for the crystallographic experiment, even though the concentration of the inhibitor is 2 orders of magnitude above the K_i (0.2 mM; Nowak & Mildvan, 1970). Refinement performed assuming 50% occupancy yielded *B*-factors comparable to those of surrounding protein atoms. Nevertheless, the position and conformation of the inhibitor are well defined. The density is elongated, implying that the molecule adopts an extended conformation. A peak 4σ high locates the phosphate group rather accurately at the end of the molecule that points away from metal site I and toward the protein surface.

Polar interactions made by the inhibitor are listed in Table 4. The phosphate oxygens hydrogen-bond with the guanidinium group of Arg 373, the hydroxyl group of Ser 36, and both the hydroxyl and the main-chain NH of Ser 374. The C_2 methylene group of phosphoglycolayte is in van der Waals contact with the His 157, Lys 344, Arg 373, and Ser 374 side chains. Ser 36 is from loop L1 in the N-terminal domain, His 157 is in loop L2, Lys 344 is in the β-turn between β_6 and α_6 in the β barrel, and Arg 373 and Ser 374 are in the β-turn between β_7 and α_7. The interaction of the phosphate group with the arginine and the two serines was

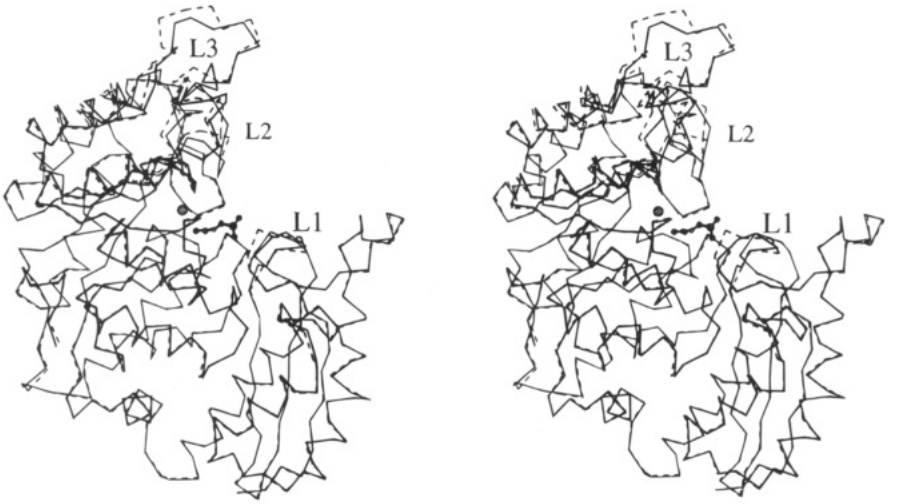

FIGURE 5: Comparison of apoenolase and the Mn^{2+}−phosphoglycolate complex. The full line is the complex. Mobile loops are labeled. Phosphoglycolate and the Mn^{2+} ion are in ball-and-stick representation. Drawn with Molscript (Kraulis, 1991).

Table 3: Manganese Coordination at Metal Site I

atom	residue	dist (Å)	B (Å^2)
OD2	Asp 244	2.39	43
OE1	Glu 294	2.40	26
OD2	Asp 319	2.27	45
OH2	Wat 441	2.05	29
OH2	Wat 442	2.26	62
OH2	Wat 443	2.13	45

also reported for the phosphonate group of phosphonoacetohydroxamate in the yeast enzyme by Wedekind et al. (1994). The interaction with the arginine, but not with the two serines, was reported for the phosphate of 2-phosphoglycerate or phosphoglycolate by Lebioda and Stec (1991) and Lebioda et al. (1991). In unligated yeast enolase, the phosphate site is occupied by a sulfate ion which interacts with both Arg 373 and Ser 374 (lobster numbering). We also find a sulfate ion at this site in the absence of a phosphorylated ligand.

At the opposite end of the phosphoglycolate molecule, the carboxylate of the inhibitor approaches the Mn^{2+} ion, but there is no continuity in the electron density and the shortest metal−oxygen distance is 4.5 Å. This precludes direct coordination, yet allows a solvent-mediated interaction. This finding is at variance with the description given by Lebioda et al. (1991) for the complex of yeast enolase with phosphoglycolate and Zn^{2+}. There, the carboxylate of the inhibitor coordinates with Zn^{2+}, possibly a consequence of the different properties of the two metals. Instead, we find the carboxylate to be in contact with the ϵ-amino group of Lys 344 and the carboxylate of Glu 209. The latter interaction implies that one of the two carboxylates is protonated.

Active Site Water Molecules and the Location of Metal Site II. There is well-defined feature (W444 in Figure 7) in the electron density of the Mn^{2+}−phosphoglycolate complex that bridges the carboxylate of the inhibitor with two other carboxylates, those of Glu 166 and Glu 209. W444 is not seen in lobster apoenolase, where the side chain of Glu 209 points away from Glu 166. Given that it has four oxygen ligands, W444 is likely to be an NH_4^+ ion rather than water in an ammonium sulfate grown crystal, yet its surroundings are also ideal for a metal site. Since W444 superimposes exactly with the water molecule noted WATB by Lebioda and Stec (1991) in the yeast enolase−Mg^{2+}−substrate complex, we modeled it as a solvent molecule rather than a metal ion. The electron density and the results of B-factor refinement suggest the presence of approximately eight electrons at this site. If it is a partly occupied Mn^{2+} site, the occupancy should be about 35%, slightly less than for phosphoglycolate. On the other hand, there is no feature in our electron density map that can safely be assigned to metal site II. There is no clear biochemical evidence that site II is occupied in the presence of phosphoglycolate. In the presence of substrate, site II has less affinity for metal ions than site I, and it binds Mg^{2+} better than Mn^{2+} (Lee & Nowak, 1992a).

In yeast enolase, contradictory crystallographic data exist on the location of metal site II. In ternary complexes with Ca^{2+}, Zn^{2+}, or Mg^{2+} and either phosphoglycolate or the substrate (Lebioda & Stec, 1991; Lebioda et al., 1991), the metal is seen at site I only. In the complexes with phosphonoacetohydroxamate and either Mn^{2+} or Mg^{2+}, two different locations of site II have been proposed. Zhang et al. (1994) placed a Mn^{2+} ion at the phosphonate end of the inhibitor, but the interpretation of the electron density there was much less certain than for site I and the coordination of the putative metal was not established. In lobster enolase, there is relatively weak density near the phosphate group of phosphoglycolate. We interpreted it as a solvent molecule, since it has no protein ligand that would fit a metal ion. As in the case of the yeast crystals, low occupancy of site II could be due to competition with ammonium ions even though the crystals were soaked in Mn^{2+} at a concentration much above the one needed for activation of the enzyme, which is in the micromolar range.

Wedekind et al. (1994) had a different crystal form grown in low salt. They located two Mg^{2+} ions sharing the keto group of phosphonoacetohydroxamate as a ligand. One ion also ligated the hydroxamic group; the other, the phosphonate. The first position fits with that of Mn^{2+} at site I in Zhang et al. (1994); the second has no equivalent in their structure. The short distance (4 Å) between the two Mg^{2+} ions in the structure of Wedekind et al. (1994) and their sharing an oxygen ligand accord to EPR data obtained with Mn^{2+} and phosphonoacetohydroxamate (Poyner & Reed, 1992). These data showed spin-exchange coupling between

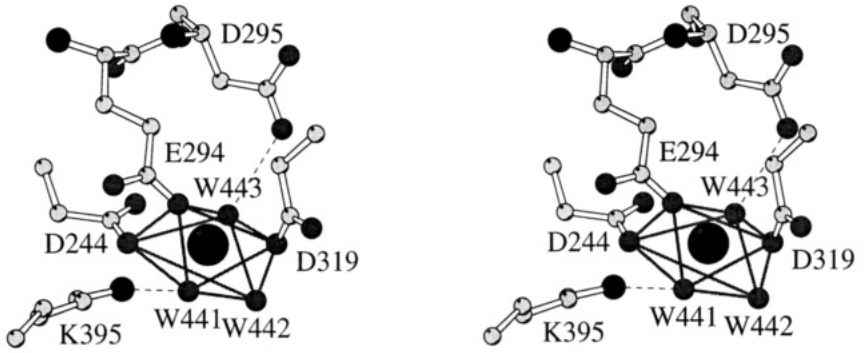

FIGURE 6: Metal site I. The Mn^{2+} ion ligates three carboxylates and three water molecules. Drawn with Molscript (Kraulis, 1991).

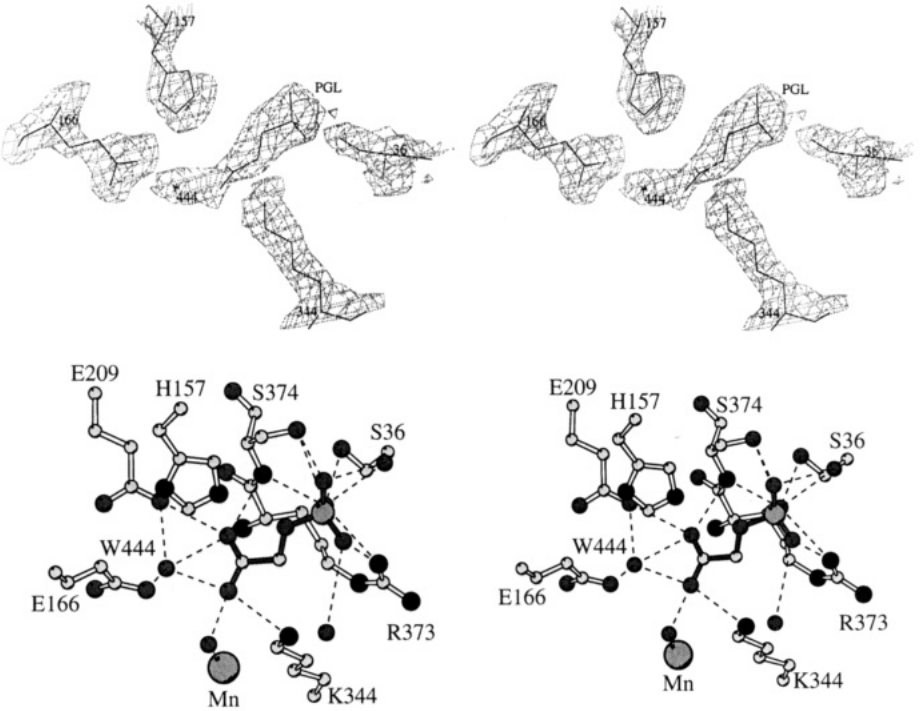

FIGURE 7: The active site with bound phosphoglycolate. (a, top) Electron density for the inhibitor and neighboring residues in a $2F_o - F_c$ map contoured at 1σ. W444 is seen bound at the left (carboxylate) end of the inhibitor. Drawn with program O (Jones et al., 1991). (b, bottom) Stereo pair drawn with Molscript (Kraulis, 1991).

Table 4: Polar Interactions Made by Phosphoglycolate and W444

atom	residue	atom	residue	dist (Å)
OP1	PGL 439	NH2	Arg 373	2.99
OP2	PGL 439	NH2	Arg 373	3.13
		N	Ser 374	3.02
		OG	Ser 36	3.13
		OG	Ser 374	3.21
		O	Wat 121	2.91
OP3	PGL 439	OG	Ser 374	2.75
		O	Wat 121	3.13
OC1	PGL 439	O	Wat 444	2.82
		N	Ser 374	3.17
		OE2	Glu 209	2.99
OC2	PGL 439	O	Wat 444	2.59
		NZ	Lys 344	2.96
		O	Wat 441	2.79
O	Wat 444	NZ	Lys 395	3.20
		OC1	PGL 439	2.82
		OC2	PGL 439	2.59
		OE2	Glu 166	2.77
		OE2	Glu 209	2.67

two metal ions, which could not occur if they were far apart as in the model of Zhang et al. (1994). However, spectroscopic data are also contradictory. The spin-exchange coupling reported with Mn^{2+} and phosphonoacetohydroxamate was not observed by Lee and Nowak (1992b) with substrate or phosphoglycolate. Rather, the EPR data suggest that the two metal sites are more than 12 Å apart in this case, while ^{31}P and ^{1}H relaxation enhancement places site II 5−7 Å from the C_2 and phosphorus atoms of the inhibitor. These data are incompatible with the location proposed by Wedekind et al. (1994) and in poor agreement with either the site next to the phosphate group proposed by Zhang et al. (1994) or the one near the carboxylate suggested above.

The Carbanion Intermediate. A compelling chemical argument for the carbanion mechanism is that yeast and muscle enolases catalyze the exchange of the α-proton of 2-phosphoglycerate with solvent faster than they do for the hydroxyl oxygen (Dinovo & Boyer, 1971; Stubbe & Abeles, 1980). Moreover, proton abstraction can be carried out independently of dehydration, since muscle enolase also catalyzes α-proton exchange on phosphoglycolate (Stubbe & Abeles, 1980). The activation barrier for proton abstraction has two components: one is the intrinsic difficulty of breaking a CH bond; the other is the difference in free energy between deprotonating either the carbon acid or the conjugate acid of the catalytic base (Figure 8). This difference ΔG_{pk}

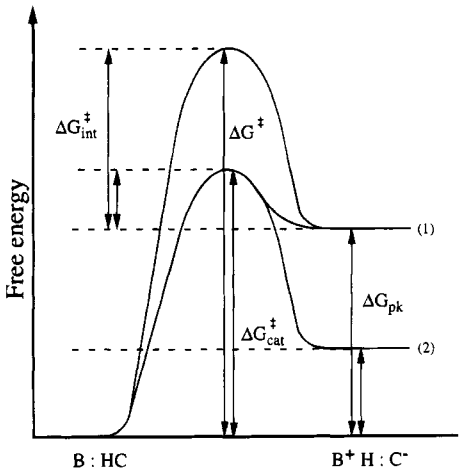

FIGURE 8: Free energy diagram and the catalysis of proton abstraction from a carbon acid. As the proton of the carbon acid is transfered to a base of much lower pK_a, the free energy gap is ΔG_{pk} and the activation energy, $\Delta G^{\ddagger}$. In the reverse direction, the uncatalyzed activation energy is $\Delta G_{int}^{\ddagger}$. A catalyst may lower the barrier to $\Delta G^{\ddagger}_{cat}$ by reducing either (1) the intrinsic activation energy $\Delta G_{int}^{\ddagger}$ or (2) the gap between the two pK_a's. We assume that enolase does both.

is directly related to the pK_a's of the two acids:

$$\Delta G_{pk} = RT \ln \Delta pK_a$$

For the carbanion mechanism to be functional in an enzyme with k_{cat} of the order of 10^2 s^{-1} at 300 K, $\Delta G^{\ddagger}$ must be less than about 15 kcal·mol^{-1}. This requires the two pK_a's to differ by less than 11 pH units, assuming $\Delta G_{int}^{\ddagger}$ to be zero. Classical studies indicate that whereas $\Delta G_{int}^{\ddagger}$ is small for oxygen or nitrogen acids, it is usually larger than 7 kcal·mol^{-1} for carbon acids (Eigen, 1964). This effectively reduces acceptable values of ΔpK_a to a narrow 0−6 range. In an enzyme, the catalytic base must perform its function near neutrality, typically at pH 7−9 in enolase, and therefore, its pK_a must be around 7 or below. As a consequence, the carbanion cannot be on the catalytic pathway unless the conjugate carbon acid has a pK_a lower than 18, taking $\Delta G_{int}^{\ddagger}$ to be zero, and possibly lower than 10 if $\Delta G_{int}^{\ddagger}$ is large. For an aliphatic CH group, these are excessively low pK_a's and a major difficulty with carbanion-based mechanisms (Thibblin & Jencks, 1979).

In principle, carbanion formation can be accelerated by either lowering the pK_a or catalyzing CH bond breaking. Most likely, enzymes do both. Gerlt and Gassmann (1993a,b) have proposed a general mechanism for lowering the pK_a of carbon acids in α to a keto group. It is based on the formation of an enolic intermediate stabilized by a short hydrogen bond to an acidic group on the protein that has the same pK_a as the enol. Such a bond is assumed to be much more stable than normal hydrogen bonds (Gerlt & Gassmann, 1992; Cleland, 1992). An enolic intermediate almost certainly occurs in triose-phosphate isomerase, which has an aldehyde as substrate (Lodi & Knowles, 1991). Enolization of an aliphatic aldehyde or ketone has an equilibrium constant of 10^{-8}−10^{-6} (Chiang & Kresge, 1991). It converts a CH acid with a pK_a of 17−20 into an OH acid with a pK_a ≈ 11, so that the proton is easily transferred to an amino acid side chain having approximately the same pK_a.

Enolase and Mandelate Racemase. Does the same mechanism apply to enzymes with less easily enolized substrates, such as carboxylates or thioesters? In citrate synthase, the thioester group of acetyl-CoA may enolize, but the idea that the enol is stabilized by short strong hydrogen bonds is not supported by high-resolution X-ray data (Usher et al., 1994). When the substrate is a carboxylate, enolization is more difficult. It yields a dianionic *aci*-carboxylate, which has been suggested to be a catalytic intermediate in mandelate racemase (Gerlt et al., 1991; Mitra et al., 1995). Mandelate racemase is probably the closest relative to enolase among known protein structures. It has a $\beta^3\alpha_4$ N-terminal domain followed by a $(\beta\alpha)_8$ barrel missing helix α_8 (Neidhart et al., 1990). The barrel is shown in Figure 9 superimposed onto that of lobster enolase. The active sites, metal sites, and some of the catalytic residues are similarly located. The $\beta_3\alpha_4$ domain alone superimposes onto that of lobster enolase with a 2.3 Å rmsd measured on 82 C_α out of 130, and it occupies a slightly different position relative to the α/β barrel.

To perform racemization, mandelate racemase abstracts the α-proton of mandelate (α-hydroxyphenylacetate) in either the *R* or the *S* position. Its active site contains two catalytic bases, a lysine and a histidine, placed on each side, and a Mg^{2+} ion. Proton abstraction is assisted by electrophilic catalysis as the carboxylate of mandelate binds the metal and possibly by acid catalysis as it also hydrogen bonds to a lysine and a glutamic acid (Lys 164 and Glu 317; Neidhart et al., 1991; Landro et al., 1994). These two hydrogen bonds resembles those made by Lys 344 and Glu 209 in lobster enolase, and here again, the direct contact between two carboxylates implies that one of them is protonated. In solution, protonating the carboxylate of the mandelate anion reduces the pK_a of its α-proton from above 30 to a value of 22, still too high. Rather than assuming that the pK_a of the bound substrate is lower, Mitra et al. (1995) propose a mechanism based on enolization with a short strong hydrogen bond to Glu 317 stabilizing an *aci*-carboxylate intermediate.

In enolase, we do not know the pK_a of the α-proton of 2-phosphoglycerate. It is certainly excessively high when the carboxylate carries a full negative charge. When the carboxylate is protonated (or neutralized by the interaction with a metal ion), the α-proton should be significantly more acidic than in acetic acid (pK_a ≈ 24; Pearson & Dillon, 1953), due to the inductive effect of the hydroxyl and phosphoester substituents. This effect should be sensitive to the charge carried by the phosphate group and therefore to its protonation state or, if Zhang et al. (1994) are right and metal site II is next to the phosphate, to the presence of a neutralizing counterion.

The Nature of the Catalytic Base. If we assume pK_a's near 17 for the α-proton and 7 for the catalytic base, there is no need for the *aci*-carboxylate to be an obligatory intermediate in enolase provided the enzyme catalyzes CH bond breaking. However, protonation of the substrate carboxylate at neutral pH requires acid catalysis, and we suggest that this is the function of water W444 or, rather, of the Glu 166−Glu 209−W444 proton relay system. Lebioda and Stec (1991) took that same water molecule to be the catalytic base taking the α-proton. This was an unlikely choice, given that its unperturbed pK_a should be below 0 (if it is H_2O) or above 15 (for OH^-). In contrast, acid catalysis requires only a small shift of the pK_a of the carboxylic acids, for which their clustering together as seen in the present X-ray structure is a sufficient explanation. Our suggestion is fully compatible with the result of site-directed mutagen-

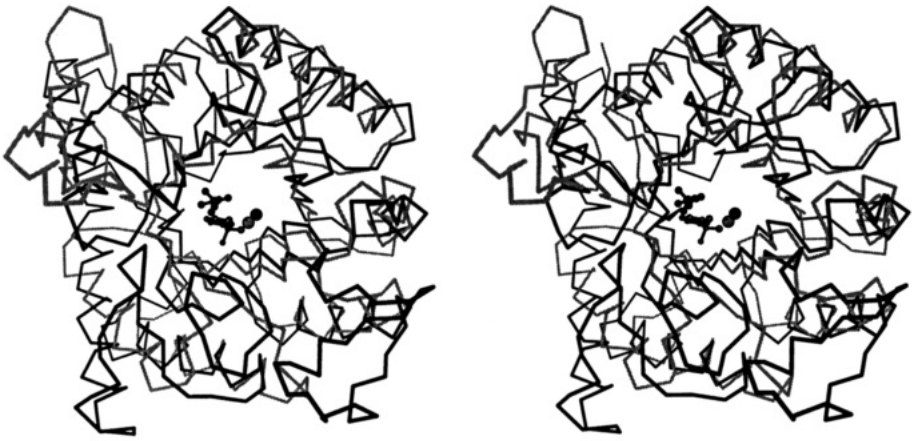

FIGURE 9: Superposition of the α/β barrels in enolase and mandelate racemase.The two barrels superimpose with a rmsd of 2.0 Å for 142 C_α excluding the atypical part of the enolase barrel. Phosphoglycolate and Mn^{2+} in enolase (dark bonds) approximately superimpose with a mandelate analogue and Mg^{2+} in complex with mendelate racemase (light bonds; Landro et al., 1994, file 1MNS). Drawn with Molscript (Kraulis, 1991).

esis of the equivalent of Glu 166 in the yeast enzyme. Substitution with a glutamine reduces activity by a factor of 10^4 (Brewer et al., 1993), which we interpret as the effect of the negative charge carried by Glu 166 on the pK_a of the substrate carboxylate. In the mutant, the pK_a should return to its normal value below 5, making α-proton abstraction more difficult.

In the Mn^{2+}−phosphoglycolate complex of lobster enolase, we find the imidazole group of His 157 to be in van der Waals contact (4.5 Å) with the C_2 atom of the inhibitor. This position is a consequence of a movement of loop L2 toward the inhibitor. In the apoenzyme, loop L2 is disordered, and there is no interpretable density for its side chains. The position of loop L2 seen in our ternary complex was also observed by Lebioda et al. (1993) in a complex of yeast enolase with phosphate and fluoride but not with phosphoglycolate or 2-phosphoglycerate. In the phosphonoacetohydroxamate−Mg^{2+} complex (Wedekind et al., 1994), the equivalent His 159 is in contact with the inhibitor and interacts with the phosphonate. Thus, at least two yeast X-ray structures confirm that loop L2 can move to a position where the histidine is at the active site.

We suggest that the catalytic base in enolase is His 157. This is at variance with the mechanism proposed by Lebioda and Stec (1991), who give no functional role to this residue, and with Wedekind et al. (1994), who proposed the equivalent of Lys 344 to be the catalytic base. A lysine with a pK_a shifted down by about 3 pH units is a plausible alternative to a histidine, but it is much less frequently used as a base in enzymic catalysis.

The decision between His 157 and Lys 344 as the base performing the first step of the dehydration reaction will presumably be made by site-directed mutagenesis. The result will also bear on the mechanism's second step, β-elimination of the hydroxyl group. Though the inhibitor used here lacks the hydroxymethyl moiety of the true substrate, the position of the missing group is fully determined by the known stereospecificity of enolase for the D enantiomer. As its elimination occurs *anti* to the C_2 proton (Cohn et al., 1970), its orientation is also determined. If the base is His 157, the hydroxyl is in position to bind to the metal at site I; if it is Lys 344, it is not. Thus, Wedekind et al. (1994) propose that the metal ligates the carboxylate instead of the hydroxyl. This interpretation, which contradicts the one Lebioda and Stec (1991) gave of their X-ray structure of a complex with the real substrate, has a weak basis since phosphonoacetohydroxamate has no carboxylate, only a keto group. Moreover, its hydroxamic group, which should mimic the hydroxyl, does bind to the metal. Phosphoglycolate, which

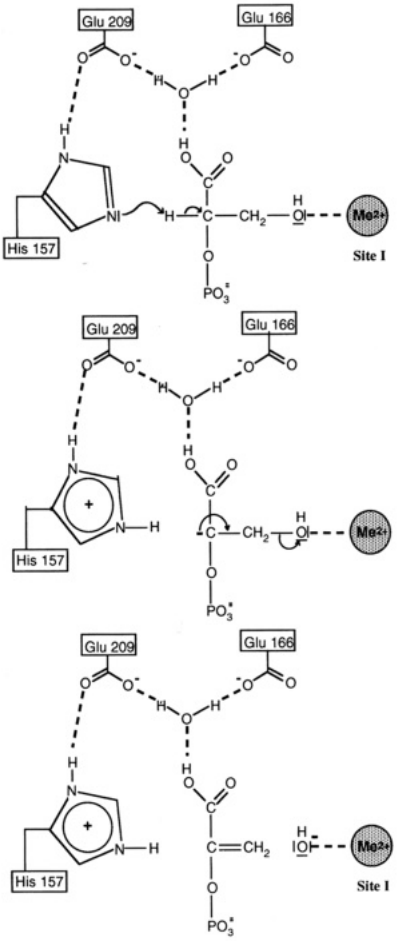

FIGURE 10: Proposed catalytic mechanism of enolase. Glu 166, Glu 209, and the water molecule form a proton relay system that allows protonation of 2-phosphoglycerate. The pK_a's of His 157 and the C_2H group differ by less than 10 pH units, allowing fast proton transfer from the carbon acid to the imidazole. The delocalized charge of the carbanion is directed toward the hydroxyl oxygen by a divalent metal at site I. The charge on the metal-bound hydroxyl ion also helps its elimination, yielding phosphoenolpyruvate.

has a carboxylate, is found here not to ligate the metal. We therefore agree with Lebioda and Stec (1991) and with a large body of biochemical evidence [reviewed by Brewer (1981, 1985)] showing that the metal at site I binds the hydroxyl group.

The Catalytic Mechanism of Enolase. Figure 10 summarizes our conclusions concerning the catalytic mechanism of enolase. It is drawn in the hypothesis where W444 is a water molecule, and it assigns no specific function to the second metal site. If, however, W444 is a metal ion, its interaction with the substrate carboxylate would make it an obvious candidate for electrophilic catalysis: it would play the same role as the single metal site in mandelate racemase, which also interacts with the caboxylate of the substrate (Neidhart et al., 1991).

In our scheme, the substrate of the reaction is in the carboxylic acid form, and His 157 is neutral when the forward reaction starts. As His 157 takes up the α-proton, the negative charge on C_2 becomes delocalized. It is distributed over several adjacent atoms, the metal at site I favoring a localization on the hydroxylmethyl oxygen rather than on the *aci*-carboxylate oxygens of an enolic intermediate as in a Gerlt−Gassmann scheme. This fits with the data of Stubbe and Abeles (1980) showing that the presence of a hydroxyl group facilitates proton abstraction. In addition to lowering the free energy of the carbanion, the charge developping on the hydroxyl should help β-elimination by weakening the C−O bond. In the reverse direction, a metal-bound hydroxyl ion performs nucleophilic attack on the ethylenic C_3 atom of phosphoenolpyruvate. Its negative charge distributes over other atoms including C_2, which takes up a proton from His 157 now in the imidazolium state.

Conclusion. The enolase mechanism shown in Figure 10 combines base catalysis, acid catalysis, and metal catalysis to accelerate a rather simple step in a major metabolic pathway. It involves no unusually strong hydrogen bonds or enolic intermediate. It diverges from the conclusions drawn by Wedekind et al. (1994) from a study using a hydroxamate inhibitor which, in spite of its very high affinity for enolase, appears not to be an analogue of the transition state. It is in agreement with Lebioda and collaborators on several points including one of the three catalytic elements: the metal. Yet, we attribute a very different role to the water molecule located at the active site and propose a histidine to be a more conventional catalytic base than water. Given the discrepancy between models of catalysis derived from high-resolution X-ray structures, it is well worth noting that Figure 10 is in full agreement with the mechanism proposed more than 20 years ago (Dinovo & Boyer, 1971; Nowak et al., 1973) and to which the present work provides a structural basis.

ACKNOWLEDGMENT

The analysis of lobster cDNA was performed by S.D. in the laboratory of Prof. M. Jacquet (Orsay). We acknowledge his help and advice and also the competent assistance of G. LeBras (Gif-sur-Yvette) in biochemical preparations. We are grateful to Prof. R. Fourme, Prof. J. P. Benoît, and the staff of LURE (Orsay) for making station W32 on the wiggler line of LURE-DCI available to us.

REFERENCES

Banner, D. W., Bloomer, A. C., Petsko, G. A., Phillips, D. C., Pogson, C. I., Wilson, I. A., Corran, P. H., Furth, A. J., Milman, J. D., Offord, R. E., Priddle, J. D., & Waley, S. G. (1975) *Nature 225*, 609−614.
Bishop, J. G., & Corces, V. G. (1990) *Nucleic Acids Res. 18*, 191.
Brewer, J. M. (1981) *CRC Crit. Rev. Biochem.*, 209−254.
Brewer, J. M. (1985) *FEBS Lett. 182*, 8−14.
Brewer, J. M., Robson, R. L., Glover, C., Holland, M., & Lebioda, L. (1993) *Proteins: Struct., Funct., Genet. 17*, 426−434.
Brünger, A. T., Kuriyan, J., & Karplus, M. (1987) *Science 235*, 458−460.
CCP4 (1979) SERC, Daresbury, Warrington, U.K.
Chiang, Y., & Kresge, J. A. (1991) *Science 253*, 395−400.
Chothia, C., & Lesk, A. (1986) *EMBO J. 5*, 823−826
Cleland, W. W. (1992) *Biochemistry 31*, 317−319
Cohn, M., Pearson, J. E., O'Connell, E. L., & Rose, I. A. (1970) *J. Am. Chem. Soc. 92*, 4095−4098
Devereux, J., Haeberli, P., & Smithies, O. (1984) *Nucleic Acids Res. 12*, 387−695.
Dinovo, E. C., & Boyer, P. D. (1971) *J. Biol. Chem. 246*, 4586−4593.
Dumas, C., & Camonis, J. (1993) *J. Biol. Chem. 268*, 21599−21605.
Dumas, C., Duquerroy, S., & Janin, J. (1995) *Acta Crystallogr. D* (in press).
Duquerroy, S., LeBras, G., & Janin, J. (1994) *Proteins: Struct., Funct., Genet. 18*, 390−393.
Eigen, M. (1964) *Angew. Chem., Int. Ed. Engl. 3*, 1.
Engh, R. A., & Huber, R. (1991) *Acta Crystallogr. A47*, 292−400.
Farber, G. K. (1993) *Curr. Opin. Struct. Biol. 3*, 409−412.
Fourme, R., Dhez, P., Benoit, J. P., Dubuisson, J. P., Besson, P. & Frouin, J. (1992) *Rev. Sci. Instrum. 63*, 982−987.
Gerlt, J. A., & Gassman, P. A. (1992) *J. Am. Chem. Soc. 114*, 5928−5934.
Gerlt, J. A., & Gassman, P. A. (1993a) *J. Am. Chem. Soc. 115*, 11552−11568.
Gerlt, J. A., & Gassman, P. A. (1993b) *Biochemistry 32*, 11943−11952.
Gerlt, J. A., Kozarich, J. W., Kenyon, G. L., & Gassman, P. G. (1991) *J. Am. Chem. Soc. 113*, 9667−9669.
Holland, M. J., Holland, J. P., Thill, G., & Jackson, K. (1981) *J. Biol. Chem. 256*, 1385−1395.
Janin, J., Miller, S., & Chothia, C. (1988) *J. Mol. Biol. 204*, 155−166.
Jones, T. A., Zou, J.-Y., Cowan, S. W., & Kjeldgaard, M. (1991) *Acta Crystallogr. A47*, 110−119.
Kraulis, P. J. (1991) *J. Appl. Crystallogr. 24*, 946−950.
Landro, J. A., Gerlt, J. A., Kozarich, J. W., Koo, C. W., Shah, V. J., Kenyon G. N., Neidhart, D. J., Fujita, S., & Petsko, G. A. (1994) *Biochemistry 33*, 635−643.
Laskowski, R. A., MacArthur, M. W., Moss, D. S., & Thornton, J. M. (1993) *J. Appl. Crystallogr. 26*, 283−291.
Lebioda, L., & Stec, B. (1988) *Nature 333*, 683−686.
Lebioda, L., & Stec, B. (1989) *J. Am. Chem. Soc. 111*, 8511−8513.
Lebioda, L., & Stec, B. (1991) *Biochemistry 30*, 2817−2822.
Lebioda, L., Stec, B., & Brewer, J. M. (1989) *J. Biol. Chem. 264*, 3685−3693.
Lebioda, L., Stec, B., Brewer, J. M., & Tykarska, E. (1991) *Biochemistry 30*, 2823−2827.
Lebioda, L., Zhang, E., Lewinski, K., & Brewer, J. (1993) *Proteins: Struct., Funct., Genet. 16*, 219−225.
Lee, B. H., & Nowak, T. (1992a) *Biochemistry 31*, 2165−2171.
Lee, M. E., & Nowak, T. (1992b) *Biochemistry 31*, 2172−2180.
Leslie, A., Brick, P., & Wonacott, A. (1986) *Daresbury Lab. Inf. Q. Protein Crystallogr. 18*, 33−39.
Lodi, P. J., & Knowles, J. R. (1991) *Biochemistry 30*, 6948−6956.
Mitra, B., Kallarakal, A. T., Kozarich, J. W., & Gerlt, J. A. (1995) *Biochemistry 34*, 2777−2778.
Neidhart, D. J., Kenyon, G. L., Gerlt, J. A., & Petsko, G. A. (1990) *Nature 347*, 692−694.

Neidhart, D. J., Howell, P. L., Petsko, G. A., Powers, V. M., Li, R., Kenyon, G. L., & Gerlt, J. A. (1991) *Biochemistry 30,* 9264–9273.
Nowak, T., & Mildvan, A. S. (1970) *J. Biol. Chem. 245,* 6057–6064.
Nowak, T., Mildvan, A. S., & Kenyon, G. (1973) *Biochemistry 12,* 1690–1701.
Pearson, R. G., & Dillon, R. L. (1953) *J. Am. Chem. Soc. 75,* 2439–2443.
Poyner, R., & Reed, G. (1992) *Biochemistry 31,* 7166–7173.
Read, R. J. (1986) *Acta Crystallogr. A42,* 140–149.
Sambrook, J., Fritsch, E. F., & Maniatis, T. (1989) *Molecular cloning: a laboratory manual,* Cold Spring Harbor Laboratory Press, Cold Spring Harbor, NY.
Stec, B., & Lebioda, L. (1990) *J. Mol. Biol, 211,* 235–248.
Stubbe, J., & Abeles, R. (1980) *Biochemistry 19,* 5505–5512.
Thibblin, A., & Jencks, W. P. (1979) *J. Am. Chem. Soc. 101,* 4963.
Usher, K. C., Remington, S. J., Martin, D. P., & Drueckhammer, D. G. (1994) *Biochemistry 33,* 7753–7759.
Wedekind, J., Poyner, R., Reed, G., & Rayment, I. (1994) *Biochemistry 33,* 9333–9342.
Wedekind, J. E., Reed, G. H., & Rayment, I. (1995) *Biochemistry 34,* 4325–4330.
Wold, F. (1971) *Enzymes, 3rd Ed. 5,* 499–537.
Zhang, E., Hatada, M., Brewer, J., & Lebioda, L. (1994) *Biochemistry 33,* 6295–6300.

BI951020U